Stellar Dynamics around Black Holes in Galactic Nuclei

S. Sridhar [1] and J. Touma [2]
[1] Inter-University Centre for Astronomy and Astrophysics
Ganeshkhind, Pune 411 007, INDIA
[2] McDonald Observatory, University of Texas, RLM 15.308, Austin, TX 78712, USA

ABSTRACT

We classify orbits of stars that are bound to central black holes in galactic nuclei. The stars move under the combined gravitational influences of the black hole and the central star cluster. Within the sphere of influence of the black hole, the orbital periods of the stars are much shorter than the periods of precession. We average over the orbital motion and end up with a simpler problem and an extra integral of motion: the product of the black hole mass and the semimajor axis of the orbit. *Thus the black hole enforces some degree of regularity in its neighborhood.* Well within the sphere of influence, (i) planar, as well as three dimensional, axisymmetric configurations–both of which could be lopsided–are integrable, (ii) fully three dimensional clusters with no spatial symmetry whatsover must have semi–regular dynamics with two integrals of motion. Similar considerations apply to stellar orbits when the black hole grows adiabatically. We introduce a family of planar, non–axisymmetric potential perturbations, and study the orbital structure for the harmonic case in some detail. In the centered potentials there are essentially two main families of orbits: the familiar loops and lenses, which were discussed in Sridhar and Touma (1997, MNRAS, 287, L1-L4). We study the effect of lopsidedness, and watch the emergence of a family of "resonant" loops, which we argue are suitable candidates for the construction of lopsided, eccentric, discs around black holes, such as in M31 and NGC 4486B.

1. Introduction

Following up on a decade of work with ground–based telescopes (cf. Kormendy 1982, 1987 and Lauer 1983, 1985), observations with the Hubble Space Telescope (HST) have clarified, and extended our knowledge of the centres of galaxies (cf. Lauer et. al 1995, Gebhardt et al. 1996). The brightness profiles are generically cuspy, and many correlations have been drawn between cusp steepness, isophote shapes, luminosities, kinematics, and other nuclear and global properties of galaxies. Most, if not all, galaxies might have central black holes (BH), massive enough to power active nuclei when there is an adequate supply of fuel (Rees 1990). About a dozen galaxies have been shortlisted as candidates for possessing central BHs (c.f. Kormendy and Richstone 1995), and the case is especially strong for our Galaxy, M31, M32, and NGC 3115. BH detection based on spectroscopy of stellar light requires careful modeling of the distribution and motions of stars

in the central regions. Set against this background of progress, our understanding of the dynamics of nuclear star clusters is quite poor. Gerhard and Binney (1985) argued that cusps and BHs will destroy box orbits (see de Zeeuw 1985 for a discussion of orbit structure of triaxial, integrable, potentials with cores), which are then replaced by chaotic orbits. They also observed that the resulting chaotic orbits are rounder, thus making it difficult to construct non-axisymmetric equilibria, a conclusion which has received great attention from Merritt (1996) who suggested that cuspy galaxies with BHs must necessarily be axisymmetric at least near the centre. Sridhar and Touma (1997) constructed, cuspy, non-axisymmetric, scale-free discs whose potentials are of Stäckel form in parabolic coordinates. The dynamics in these potentials is fully integrable. A BH could be added at the centre without affecting the integrability of motion. Discs without a BH support only bananas. The BH stabilizes a box-like family of orbits, the lenses. These models, as they questioned the implicit assumption that cusps and BHs imply chaos, perked our interest in further investigating dynamics very close to the BH. Here, we explore another route to more regular dynamics in galactic nuclei.

The orbits of stars in galactic nuclei are controlled by the combined gravitational forces of the central BH, and the self gravity of the cluster. Very close to the BH, the orbits are nearly Keplerian—stars bound to the BH move on nearly elliptical orbits, whereas very energetic ones whiz by hyperbolically (we ignore relativistic effects, so our discussion is applicable only to distances beyond several Schwarzschild radii from the BH). If the velocity dispersion in the cluster is σ, we might say that a BH of mass M has a strong influence on stellar orbits inside a sphere of radius, $r_h \sim GM/\sigma^2$. For fiducial values, $M \sim 10^8\,\mathrm{M}_\odot$, $\sigma \sim 100\,\mathrm{km\,s^{-1}}$, we obtain $r_h \sim 50\,\mathrm{pc}$, a spatial scale that HST with a resolution of $0.''1$ can easily resolve much farther than Virgo.[1] Keplerian ellipses do not precess, and we might expect that orbits that are strongly influenced by the BH might support asymmetric, even lopsided structures. Such appears to be the case for M31 and NGC4486B, both of which have double nuclei (Lauer et.al. 1993, 1996); these might be signatures of eccentric nuclear stellar discs (Tremaine 1995). A few other galaxies with central asymmetric light distributions are discussed in Lauer et.al. (1995). As Lauer et.al. (1996) observe, " A thorough understanding of the dynamics of eccentric disks might allow us to estimate the BH mass directly from the disk shape by relating the scale at which the disc symmetry is broken to the hole mass."

In this paper, we develop a perturbative approach toward classification of orbits within the BH sphere of influence, taking advantage of the super–integrability (i.e. degeneracy) of the Kepler problem. Borrowing an averaging technique from planetary dynamics, we introduce slow dynamics of precessional motions in § 2, and discuss integrability of slow dynamics in two, and three dimensional motions, for both time independent potentials, as well as the case when the

[1] It should be noted that σ itself is often not independent of distance from the BH, thereby confusing the significance of r_h. Perhaps a better estimate of the sphere of influence of the BH is the radius at which the mass of the cluster equals the mass of the BH.

mass of the BH grows adiabatically. We introduce a family of planar potentials that are, in general, cuspy, non–axisymmetric and lopsided. The harmonic case is particularly amenable to simple, analytic treatment, and we devote § 3 to an exploration of orbits in non–axisymmetric, and lopsided cases; orbit families that might have relevance to double nuclei are briefly discussed. Centred non harmonic perturbations, with small non–axisymmetry are considered in § 4. § 5 is devoted to outlining the limits of applicability of the averaging principle, emergence of resonant families, and the outbreak of chaos. § 6 provides a summary of our results, paying some attention to the applicability of the averaging technique to M31 and NGC 4486B.

2. Slow dynamics

Let the BH be located at the origin, and consider a cluster of stars orbiting around it. A typical stellar orbit is determined by the Hamiltonian,

$$\mathcal{H} = \frac{v^2}{2} - \frac{GM}{r} + \Phi(r) \tag{1}$$

where $\boldsymbol{r}$ and $\boldsymbol{v}$ are the position vector and velocity of the star, and Φ is the (time independent) mean gravitational potential of the cluster. If Φ were zero, the radial and azimuthal frequencies of the orbit are equal, and orbits are pure, Keplerian ellipses. Within the BH sphere of influence, Φ, by definition, is a small perturbation that makes the Keplerian ellipses precess and deform on time scales that are slow compared to orbital times. Hence it is useful to imagine that each star is a slowly precessing elliptical ring, with its mass distributed inversely proportional to its speed around its orbit—in the planetary context, this idea derives from Gauss (see Hagihara (1971) for a discussion of Gauss's idea and its applications). Rauch and Tremaine (1996) introduced it to explore relaxation effects in star clusters around supermassive BHs. The elliptical ring approach emerges naturally in the averaging process we discuss below.

When there is a separation of time scales, and one is interested in the slow evolution, it makes sense to average over high frequency variations: thus, time averages of physical quantities are equated to their space averages, an idea that has its roots in the works of Laplace, Lagrange and Gauss. The cleanest way to do this is to express the problem in appropriate action–angle variables, identify the fast and (the two) slow angles, and integrate over the fast angle. Then the conjugate (fast) action is predicted to have no secular evolution[2] In practice, resonances between fast and slow motions stand in the way of this naive averaging procedure. Such resonances are the seeds of chaos, which we explore later using surfaces of section.

To apply the averaging principle, it is convenient to cast the Kepler problem in terms of the Delaunay action–angle variables: we write these as $(I, L, L_z; w, g, h)$, where (I, L, L_z) are action

[2]Laplace did this for the solar system, and concluded that the semi–major axes of the Keplerian ellipses of the planets do not evolve secularly. It is no surprise that we get an identical result; we use it to classify stellar orbits in galactic nuclei.

variables, and (w, g, h) are the respective conjugate angle variables.[3] We list the basic definitions below, and refer the reader to text books (c.f. Plummer 1960, Goldstein 1985) for the derivation.

$$\begin{aligned} I &= \sqrt{GMa}\,, \quad \text{where } a \text{ is the semi–major axis.} \\ w &= \textit{mean anomaly}\text{, which is a measure of time along the orbit;} \\ &\quad \text{it is 0 at pericentre and advances by } 2\pi \text{ in one circuit.} \\ L &= \text{magnitude of the angular momentum; } L \le I\,. \\ g &= \text{angle from the ascending node to the pericentre.} \\ L_z &= z\text{–component of angular momentum.} \\ h &= \text{angle from } x\text{–axis to ascending node.} \end{aligned} \tag{2}$$

Expressed in the Delaunay variables, the Hamiltonian for the Kepler problem (equation 1 with Φ set equal to zero) assumes the simple form, $H_{\rm kep} = -(G^2M^2/2I^2)$. Thus w advances at a uniform rate,

$$\Omega(I) \equiv \left(\frac{dw}{dt}\right)_{\rm kep} = \frac{\partial H_{\rm kep}}{\partial I} = \frac{(GM)^2}{I^3}\,, \tag{3}$$

whereas the other five Delaunay variables remain constant.

Let us assume that we have managed to express Φ in terms of the new variables. Then the full Hamiltonian,

$$\mathcal{H} = -\frac{1}{2}\left(\frac{GM}{I}\right)^2 + \Phi\,, \tag{4}$$

where, with some abuse of notation, we now regard Φ as a function of all six Delaunay variables. For a general perturbation, the only conserved quantity is $\mathcal{H}$. The angles advance at rates given by

$$\frac{dw}{dt} = \Omega(I) + \frac{\partial\Phi}{\partial I}\,, \qquad \frac{dg}{dt} = \frac{\partial\Phi}{\partial L}\,, \qquad \frac{dh}{dt} = \frac{\partial\Phi}{\partial L_z}\,. \tag{5}$$

When Φ is small, Ω is the fastest frequency in the problem; thus w varies in time much faster than g and h, and averaging simply means that we can integrate the Hamiltonian of equation (4) over one circuit of w—this is equivalent to treating a star as an elliptical ring. The averaged Hamiltonian,

$$\overline{\mathcal{H}} = \oint \frac{dw}{2\pi}\,\mathcal{H} = \oint \frac{d\eta}{2\pi}\left(1 - \sqrt{1-(L/I)^2}\,\cos\eta\right)\mathcal{H} = -\frac{1}{2}\left(\frac{GM}{I}\right)^2 + \overline{\Phi}\,, \tag{6}$$

governs the slow dynamics of precessional motions. Since $\overline{\mathcal{H}}$ is independent of w, we recover Laplace's result that I is conserved by the slow dynamics. Furthermore, $\overline{\Phi}$ itself is another slow

[3] it is unfortunate that the notation employed by planetary dynamicists overlaps so heavily with those commonly used by galactic dynamicists for other physical quantities. Our notation is non standard, but we hope that it minimizes confusion.

integral of motion.[4] Without further ado, we can reach some general conclusions about slow dynamics in the region $r \ll r_h$. Below we list our conclusions in order of increasing generality:

1. For razor–thin discs, motion is confined to the $z = 0$ plane. Any $\Phi(x, y)$ has the two slow integrals of motion, I and $\overline{\Phi}$. Hence the slow dynamics for two dimensional potentials, however non–axisymmetric or lop–sided, is integrable, and a straightforward classification of orbits is possible.

2. For axisymmetric Φ in three dimensions, L_z is an exact integral of motion (since Φ is independent of h). We now have three integrals of motion (L_z, I and $\overline{\Phi}$), and the slow dynamics is again fully integrable.

3. In three dimensions, when Φ has no symmetry whatsoever, we still have the integrals I and $\overline{\Phi}$. The slow motion can be chaotic, but it is clear that the chaos is confined —for instance, there can be no Arnold diffusion for the slow dynamics.

2.1. Adiabatic growth of the BH

Averaging is also applicable to time dependent perturbations, $\Phi(\boldsymbol{r}, t)$, when the time variations are slower than the orbital times; as before, $I = \sqrt{GMa}$ is a quasi–invariant. In some scenarios of the formation and subsequent growth of the BH, its mass increases adiabatically (Peebles 1972, Young 1980); conservation of I implies that semi–major axis shrinks in proportion to the growth of M. When the growth time is also much longer than the precessional timescales, additional (adiabatic) invariants might arise. These will, in general, be related to the actions corresponding to precessional degrees of freedom (L, L_z, g, h). We again consider cases with different spatial symmetry.

(1) For razor–thin discs, the conserved actions are I and $\oint L dg$, where the integral is performed at fixed time, over one cycle of motion in the $L - g$ plane.

(2) For three dimensional, axisymmetric cases, in addition to I and $\oint L dg$, we have L_z as an exactly conserved quantity.

(3) For configurations that have no spatial symmetry, I is in general the only conserved quantity, since resonances or precessional chaos might destroy the other adiabatic invariants.

It is difficult to make further progress without taking into account the self–consistent evolution of the cluster potential.

---

[4] $\mathcal{H}$ is, of course, exactly conserved, but this does not give us any extra conserved quantities after averaging.

2.2. Slow planar dynamics

For razor–thin discs, orbits are restricted to the $x-y$ plane (I, w) determine the semimajor axis and position on the orbit and (L, g) the eccentricity and orientation of the ellipse in the plane. The only difference from the three dimensional case is that we allow L to take both $\pm$ values. It proves convenient to set $w = \eta - e\sin\eta$, where η is the eccentric anomaly, and e is the eccentricity given by $e^2 = [1-(L/I)^2] \leq 1$. If we imagine cartesian coordinates, $(x^{'}, y^{'})$, centred at the origin, such that positive $x^{'}$ is along the major–axis toward the pericentre, and $y^{'}$ is parallel to the minor–axis, we have $x^{'} = a(\cos\eta - e)$, and $y^{'} = a\sqrt{1-e^2}\sin\eta$. The primed coordinates being rotated by angle g with respect to the fixed coordinates, (x, y), we obtain

$$\begin{aligned} x &= a\left\{\cos g\left(\cos\eta - \sqrt{1-\ell^2}\right) - \ell\sin g\,\sin\eta\right\} \\ y &= a\left\{\sin g\left(\cos\eta - \sqrt{1-\ell^2}\right) + \ell\cos g\,\sin\eta\right\}, \end{aligned} \tag{7}$$

where $\ell = L/I$ is a dimensionless angular momentum which takes values, $-1 \leq \ell \leq 1$.

Let μ be a characteristic oscillation frequency of a test particle in the potential $\Phi(\boldsymbol{r})$, when the BH is absent. We could, for instance, take μ to be the orbital frequency of closed orbits allowed by Φ. Since this frequency will depend only on the size of the orbit, we could replace the size by a, and regard μ to be a function only of I. Then the ratio, $\delta(I) \equiv \mu/\Omega$ is a convenient small parameter for slow dynamics. We now use a dimensionless time, $\tau = \mu t$, as an appropriate measure of the slow dynamics. Defining the dimensionless, averaged Hamiltonian,

$$H(\ell, g; I) = \frac{\overline{\Phi}}{I\mu} = \oint \frac{dw}{2\pi}\left(\frac{\Phi}{I\mu}\right) = \oint \frac{d\eta}{2\pi}\left(1-\sqrt{1-\ell^2}\cos\eta\right)\left(\frac{\Phi}{I\mu}\right), \tag{8}$$

the equations of motion take the standard form,

$$\dot{\ell} \equiv \frac{d\ell}{d\tau} = -\frac{\partial H}{\partial g}, \qquad \dot{g} \equiv \frac{dg}{d\tau} = \frac{\partial H}{\partial \ell}. \tag{9}$$

In fact, much of the qualitative picture of the orbit families can be gleaned by looking at the contour plot of H in the (g, ℓ) plane (for any choice of the constant I).

2.3. A family of planar model potentials

To develop some analytic understanding of orbital structure, we introduce a family of planar potential perturbations that allow for both non–axisymmetry and lopsidedness.[5] Let us define a

[5] In the lopsided cases, the potential exerts a force on the BH, so we should imagine that the BH is 'nailed' down. It is possible to improve the situation by including cubic and higher order terms in the potential, but at the cost of considerably more complexity. We decided to forgo this luxury, since our primary goal in this paper is to pick out interesting orbits.

quadratic form,

$$q^2 \;=\; (x-d_1)^2 + \frac{(y-d_2)^2}{b^2}\,, \tag{10}$$

and the family of planar potentials,

$$\Phi(x,y) = \begin{cases} \mathrm{sgn}\,(\alpha)\Phi_0\, r_0^{-\alpha}\,(q^2+r_c^2)^{\alpha/2}\;, & \alpha \neq 0\,; \\ (\Phi_0/2)\log\,(q^2+r_c^2)\;, & \alpha = 0\,, \end{cases} \tag{11}$$

The potentials depend on the five structural parameters, $(\,\mathbf{d}, r_c, b^2, c^2, \alpha\,)$, and a magnitude parameter $(\Phi_0\, r_0^{-\alpha})$. The potentials are centred at a point that is displaced from the BH by $\mathbf{d} \equiv (d_1, d_2)$. Potential isocontours have a core of radius r_c, and constant axis ratio, b. The exponent α is a measure of the potential gradient across the contours; we require $2 \geq \alpha > -1$, a range that includes homogeneous cores as well as very centrally concentrated mass distributions. The potentials are lopsided for non zero $\mathbf{d}$, and are cuspy when $r_c = 0$. When both $\mathbf{d} = \mathbf{0}$ and $r_c = 0$, the dynamics itself is scale–free, so we may set $a = 1$. Lopsided potentials are not scale–free, even when $r_c = 0$; this is because the lopsidedness sets a scale (d). The magnitude, $(\Phi_0\, r_0^{-\alpha})$ measures the slowness of the dynamics. Specifically, we choose units such that $\mu = (\Phi_0 a^\alpha / I r_0^\alpha) = (\Phi_0 a^\alpha / \sqrt{GMa}\, r_0^\alpha)$. As discussed above, the small parameter is $(\mu/\Omega) \propto a^{(1+\alpha)}$; since $\alpha > -1$, averaging is a very good approximation for small a.

3. Planar harmonic perturbations

The slow dynamics of *harmonic* perturbations, for which $\alpha = 2$, can be studied exactly for arbitrary non–axisymmetry, and lopsidedness. The core radius loses dynamical significance in this case, so in our explorations of harmonic perturbations, we set $r_c = 0$:

$$\frac{\Phi_2}{I\mu} = \frac{1}{a^2}\left(d_1^2 + \frac{d_2^2}{b^2} - 2d_1 x - 2\frac{d_2 y}{b^2} + x^2 + \frac{y^2}{b^2}\right)\,. \tag{12}$$

Substituting for x and y, the expressions given in equations (7), gives us the perturbation explicitly in terms of the Delaunay variables. We then average over w, and obtain the following expression for the slow Hamiltonian:[6]

$$H = -\frac{3}{2}\left(1+\frac{\epsilon}{2}\right)\ell^2 \;-\; \frac{5\epsilon}{4}\left(1-\ell^2\right)\cos 2g \;+\; 3\sqrt{1-\ell^2}\left(\frac{d_1}{a}\cos g + (1+\epsilon)\frac{d_2}{a}\sin g\right)\,, \tag{13}$$

where we have introduced $\epsilon = (b^{-2}-1)$ as a measure of non–axisymmetry. The parameter space is 3 dimensional, $(\epsilon,\ d_1/a\ ,\ d_2/a\ )$, so that the slow dynamics of even planar, harmonic perturbations is quite rich. Below we study a few cases.

---

[6] A term, $\left[(5/2) + (5\epsilon/4) + (d_1/a)^2 + (1+\epsilon)(d_2/a)^2\right]$, has been dropped in the slow Hamiltonian, because it is does not contribute to slow dynamics.

3.1. Centred harmonic perturbation: $d_1 = d_2 = 0$

The simplest case is a centred ($d_1 = d_2 = 0$) perturbation, for which we may without loss of generality, set $\epsilon \geq 0$. The Hamiltonian is

$$H = -\frac{3}{2}\left(1 + \frac{\epsilon}{2}\right)\ell^2 \; - \; \frac{5\epsilon}{4}\left(1 - \ell^2\right)\cos 2g\,, \tag{14}$$

and the equations of motion are,

$$\begin{aligned} \dot{\ell} &= -\frac{\partial H}{\partial g} = -\frac{5}{2}\epsilon\left(1-\ell^2\right)\sin 2g \\ \dot{g} &= \frac{\partial H}{\partial \ell} = -3\left(1+\frac{\epsilon}{2}\right)\ell \; + \; \frac{5\epsilon}{2}\ell\cos 2g\,, \end{aligned} \tag{15}$$

When $\epsilon = 0$, the full Hamiltonian is axisymmetric and the angular momentum is an exactly conserved quantity. The orbits are the rosette–like figures given in standard text books on classical mechanics. The averaged description, of course, coincides with this picture; $H = -3\ell^2/2$, the isocontours of which are simply lines of constant ℓ in the (g, ℓ) plane. These *loop* orbits are now viewed as Keplerian ellipses that precess at a rate, $\dot{g} = -3\ell$.

When $\epsilon \neq 0$, the non–axisymmetry gives birth to a new family of orbits, the *lenses*. Figures 1a shows contour plots of H for the case $\epsilon = 0.25$, for which the isocontours of the perturbation have axis ratio $b \simeq 0.9$. The lenses are parented by the short axis orbits, which appear as the stable fixed points located at $(\pi/2, 0)$ and $(3\pi/2, 0)$. Figure 1b shows a lens orbit (for $H = -0.13$); ℓ oscillates about zero, whereas g librates about the short axis. When the lens is aligned along the short axis, it is maximally round, and when the pericentre reaches its maximum deviation from the short axis, the lens elongates to a line ("radial orbit"); its angular momentum now switches sign, and the lens returns to maximal roundness at $g = \pi/2$, but with the opposite sign of ℓ. Unlike lenses, loops have a definite sign for ℓ, and g circulates through 2π in one period. The loop in Figure 1c is a deformed rosette that spends somewhat more time near the long axis, as it circulates around the origin. The unstable fixed points at $(0, 0)$ and $(\pi, 0)$ correspond to the long axis orbits. Loops are separated from lenses by the separatrix that straddles the unstable fixed points. The separatrix orbit, as well as the loops and lenses that are close to it spend a lot of time in the vicinity of the long axis. As ϵ increases, lenses occupy an increasingly larger fraction of phase space (see Figure 1d).

When $g = n\pi$, equations (15) imply that $\dot{\ell} = 0$ and $\dot{g} = (\epsilon - 3)\ell$. Thus, when $\epsilon = 3$, $g = 0, \pi$ are *lines* of fixed points in the (g, ℓ) plane. In fact, when $\epsilon = 3$, the region occupied by the short–axis lenses has expanded to its fullest, squeezing the loops out of existence. This value of ϵ corresponds to axis ratio of two (for the isocontours of the harmonic perturbation), a case for which the full Hamiltonian is exactly integrable (see Appendix A for details). For $\epsilon > 3$, loops are completely absent, and all of phase space is populated by lenses (see Figure 2a). The long–axis orbits now become stable, and parent families of *long–axis lenses*, one of which is shown

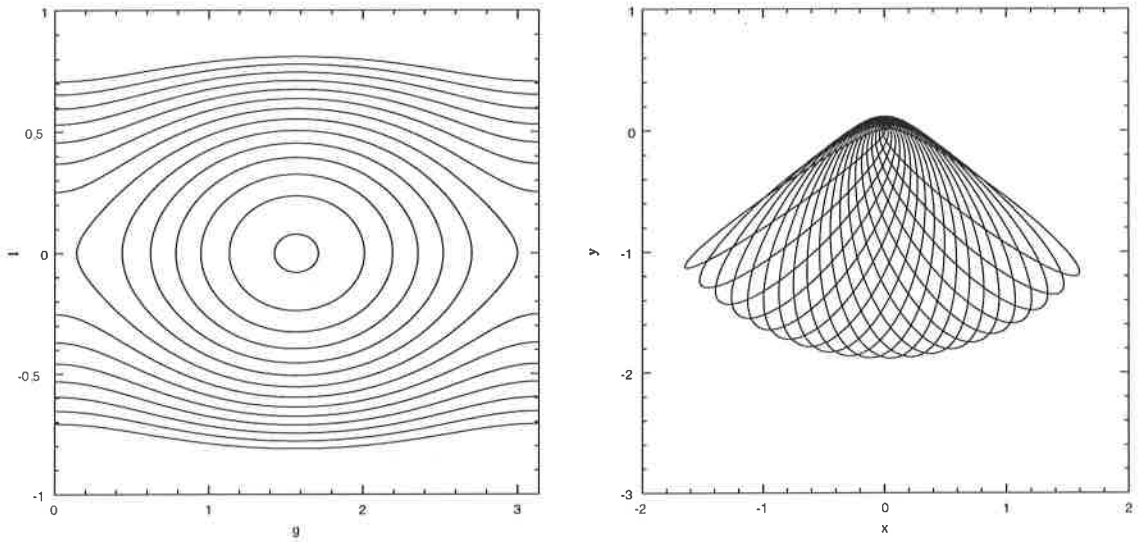

Fig. 1.— Planar, centred, harmonic perturbation: (a) isocontours of H in the (g, ℓ) plane for $\epsilon = 0.25$, (b) a lens orbit in real space corresponding to $H = -0.13$, (c) a loop orbit in real space corresponding to $H = -0.47$, (d) isocontours of H in the (g, ℓ) plane for $\epsilon = 1$

in Figure 2b. We can demonstrate this change in stability of the long–axis orbit, by expanding the H of equation (14) to lowest order about the fixed point $(0,0)$:

$$H \;=\; -\frac{5}{4}\epsilon + (\epsilon - 3)\,\frac{\ell^2}{2} + \frac{5\epsilon}{2}\,g^2\,. \tag{16}$$

When $\epsilon < 3$, the coefficients of ℓ^2 and g^2 are of opposite signs (the long–axis orbit is unstable), and have the same sign for $\epsilon > 3$ (when the long–axis orbit is stable). We can also see that the short–axis orbit remains stable by expanding H about $(\pi/2, 0)$. With $g = \pi/2 + \delta g$,

$$H \;=\; \frac{5}{4}\epsilon - (4\epsilon + 3)\,\frac{\ell^2}{2} - \frac{5}{2}\epsilon\,(\delta g)^2\,. \tag{17}$$

The coefficients of both ℓ^2 and $(\delta g)^2$ have the same sign, so the short–axis orbit is always stable.

3.2. Lopsided harmonic perturbation: $d_1 \neq 0$, $d_2 = 0$, $\epsilon = 0$

New orbits emerge when the centre of the perturbation is displaced from the BH. The simplest case occurs for $\epsilon = 0$, for which the isocontours of the perturbing potential are circles. In this case we may, without loss of generality, set $d_2 = 0$, and let $d_1 = d$. The Hamiltonian,

$$H \;=\; -\frac{3}{2}\,\ell^2 \;+\; 3\,\frac{d}{a}\sqrt{1-\ell^2}\,\cos g\,. \tag{18}$$

now has a $(\cos g)$ term, which distinguishes between orbits that are *aligned* with, from those that are *anti–aligned* with the lopsidedness of the perturbation. We recall that g is the angle from the major (x) axis to the pericentre of the instantaneous Keplerian ellipse. Thus orbits with $g = \pi$ are aligned, whereas $g = 0$ are anti–aligned with the lopsidedness. The only free parameter in H is d/a, which may be thought of as a dimensionless measure of lopsidedness. Below we explore the orbital structure as a function of this parameter.

The panels in Figures 3 show the dependence of the isocontours of H on lopsidedness. Changes in the topology of isocontours occur when d/a crosses 0.5 (Figure 3a to 3b) to and again when d/a crosses unity (Figure 3c to 3d). This behavior is best understood by following the location and stability of the fixed points. The equations of motion are,

$$\begin{aligned} \dot{\ell} \;&=\; -\frac{\partial H}{\partial g} \;=\; 3\frac{d}{a}\sqrt{1-\ell^2}\,\sin g \\ \dot{g} \;&=\; \frac{\partial H}{\partial \ell} \;=\; -3\ell \;-\; 3\,\frac{d}{a}\,\frac{\ell}{\sqrt{1-\ell^2}}\,\cos g\,, \end{aligned} \tag{19}$$

and the fixed points are determined by requiring $\dot{\ell} = \dot{g} = 0$. There are four fixed points, located at

$$\begin{aligned} g \;&=\; 0\,, \quad \ell \;=\; 0\,, \qquad \text{(anti–aligned radial orbit);} \\ g \;&=\; \pi\,, \quad \ell \;=\; 0\,, \qquad \text{(aligned radial orbit);} \\ g \;&=\; \pi\,, \quad \ell \;=\; \pm\sqrt{1-\frac{d^2}{a^2}}\,, \qquad \text{(aligned loop orbits).} \end{aligned} \tag{20}$$

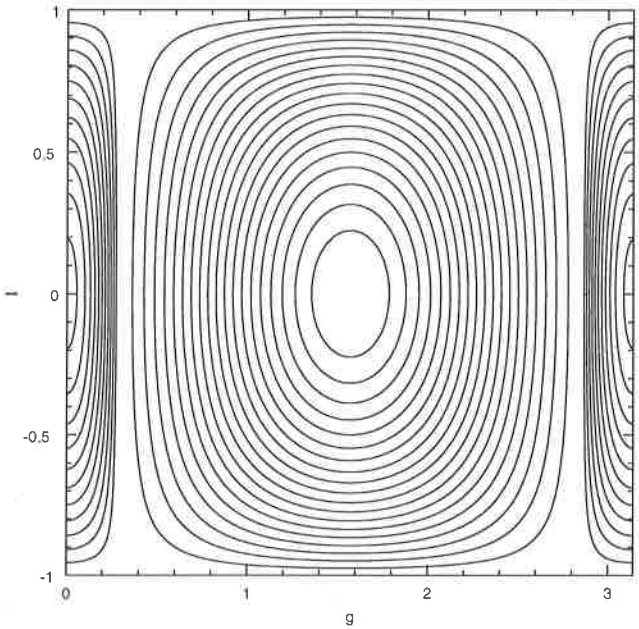

(*a*)

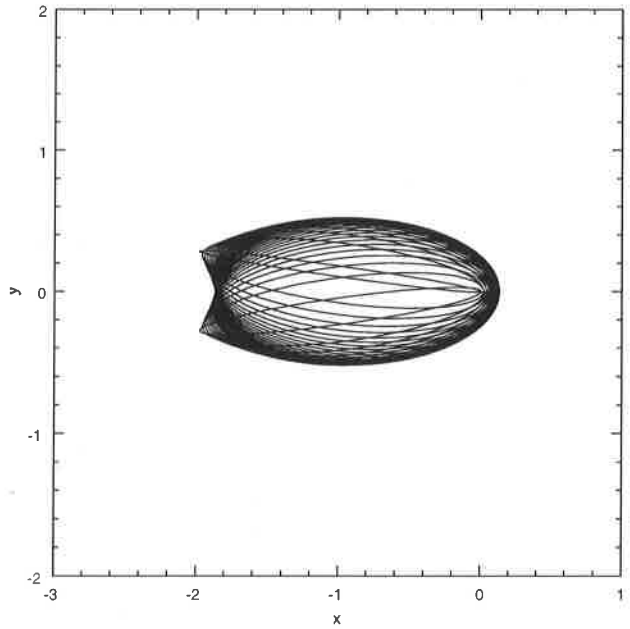

(*b*)

Fig. 2.— Planar, centred, harmonic perturbation: (a) isocontours of H for $\epsilon = 5.0$, (b) A long–axis lens orbit, for $H = -6.0$.

As Figures 3 show, the anti–aligned, radial orbit is a stable fixed point. The stability can be established by expanding H to lowest order about $(0,0)$:

$$H \;=\; 3\frac{d}{a} - \frac{3}{2}\left(1+\frac{d}{a}\right)\,\ell^2 - \frac{3}{2}\frac{d}{a}\,g^2 + \ldots\,. \tag{21}$$

The coefficients of ℓ^2 and g^2 have the same sign, so the fixed point is stable.

For $d < 0.5a$, as in Figure 3a, when one leaves the anti-aligned lenses, one first encounters rosette like loops. These orbits have a definite sense of circulation, anti–clockwise or clockwise accordingly as ℓ is $\pm$. As the average value of $|\ell|$ increases, we explore this family of loops until we go past that rosette which at $g = 0$ has $\ell = 1$. This is a critical orbit, beyond which we enter the region occupied by the more interesting family of aligned loops, a family which we explore further down. At d increases to $0.5a$, the separatrix, which bounds anti-aligned lenses away from rosettes, grows to its maximum allowable half-width of 1, squeezing the rosettes out of existence. As can be seen in Figure 3b, for which $d/a = 0.6$, the rosettes have disappeared. What about the other fixed points? They correspond to orbits that are aligned with the lopsidedness. The aligned loops have eccentricity, $e = d/a$; they begin as circular orbits when $d = 0$, elongate with increasing lopsidedness, reducing to radial orbits when $d = a$. For $d/a < 0.5$ the aligned loops are separated from the anti-aligned lenses by the rosettes. As d/a increases beyond 0.5, and while $d/a < 1$ the family of aligned loops shrinks, and is now separated from the anti-aligned lenses by lens like orbits surrounding the aligned radial orbit. All through this variation of d from 0 to $d = a$, the aligned radial orbit is unstable. At $d = a$, the two aligned loops (with either sign of ℓ) merge with the aligned radial orbit, which now remains stable for $d > a$. Again, this change of stability of the aligned, radial orbit may be verified by expanding the Hamiltonian about $(\pi, 0)$. Setting $g = \pi + \delta g$, to lowest order,

$$H \;=\; -3\frac{d}{a} \;-\; \left(1-\frac{d}{a}\right)\,\frac{3\ell^2}{2} \;+\; \frac{3}{2}\frac{d}{a}(\delta g)^2 + \ldots\,. \tag{22}$$

When $d < a$, the coefficients of ℓ^2 and $(\delta g)^2$ have opposite signs (fixed point unstable, but have the same sign for $d > a$ (fixed point stable). Hence there are three kinds of fixed points:

1. The anti–aligned radial orbit is stable for all d/a. This parents a family of *anti–aligned lenses* (see Figure 4a).

2. The aligned radial orbits are stable when $d > a$, and parents a family of *aligned lenses* (see Figure 4d).

3. The aligned loop orbits are stable when $d < a$. These parent a family of *librating loops*, to be discussed in some detail below.

There are no orbits that correspond to anti–aligned loops.

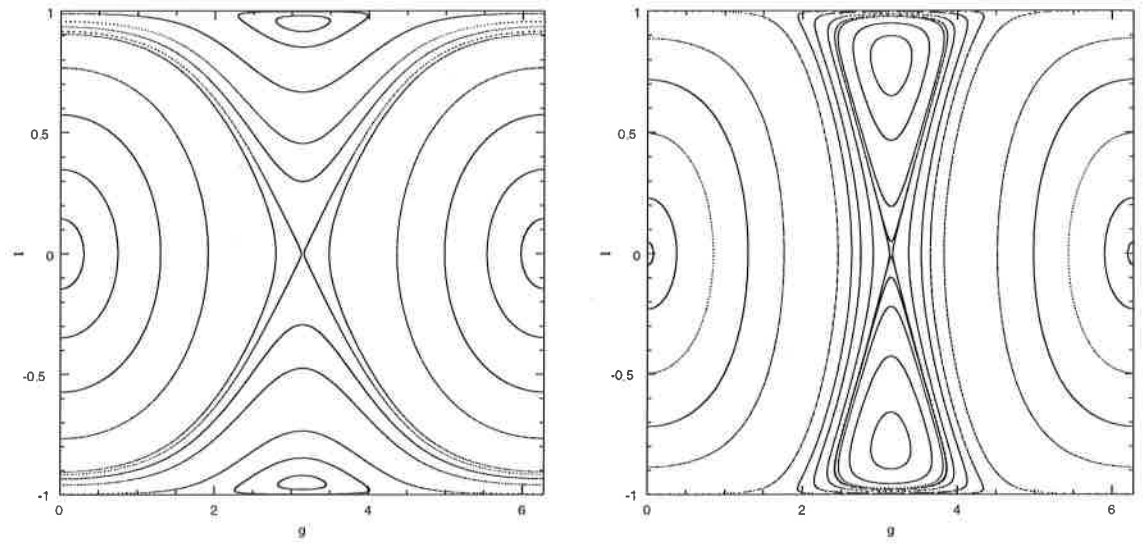

(a) (b)

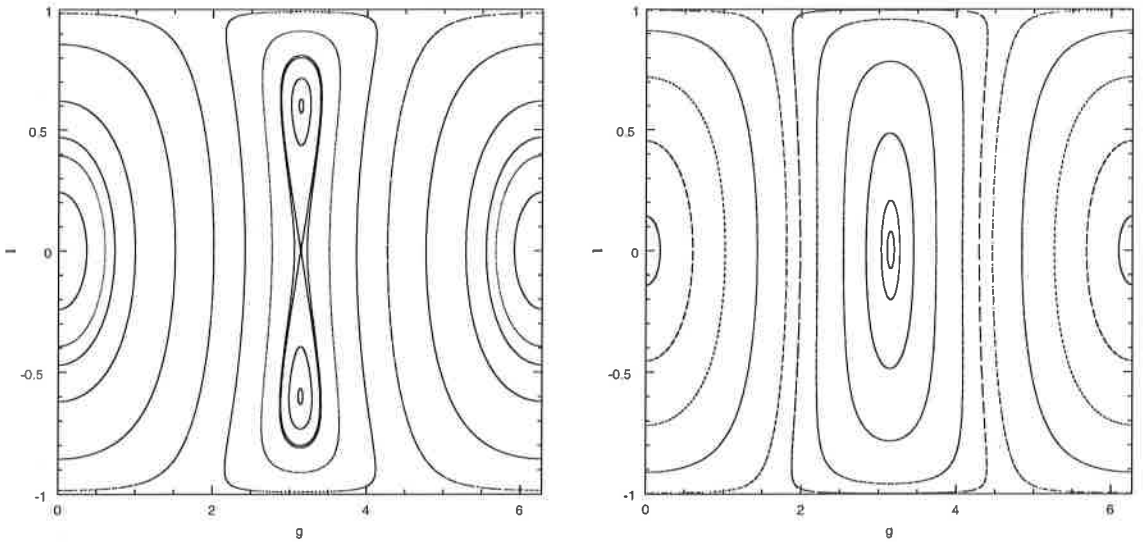

(c) (d)

Fig. 3.— Isocontours of H for planar, lopsided, harmonic perturbation (a) $d = 0.3a$, (b) $d = 0.6a$, (c) $d = 0.8a$, (d) $d = 1.5a$.

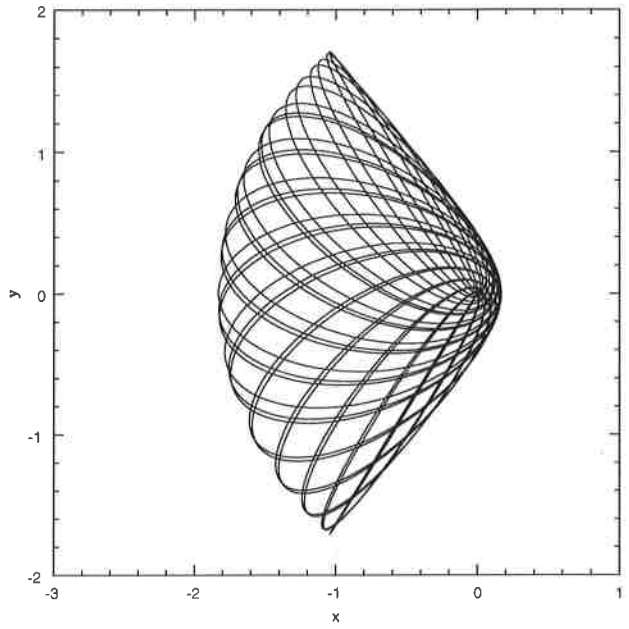

(*a*)

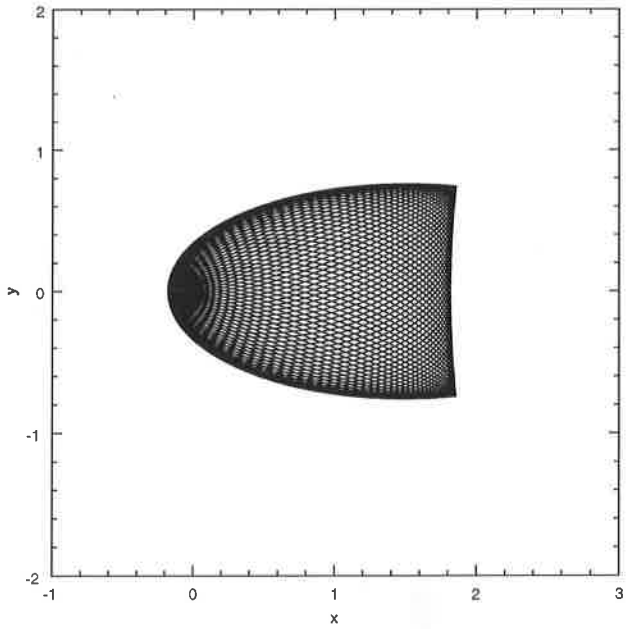

(*b*)

Fig. 4.— Lens orbits for the planar, lopsided, harmonic perturbation: (a) an anti–aligned lens orbit for $a = 1$, $d = 0.5$, (b) an aligned lens orbit for $a = 1$, $d = 1.5$.

3.3. Possible applications to lopsided galactic nuclei

The lenses and loops of (2) and (3) are orbits of different sizes: for given d, the former are smaller, with $a < d$, whereas the latter have $a > d$. However, the apocentres of both orbits librate about the line joining the BH to the centre of the perturbation. This property makes them candidate orbits for the construction of lopsided discs around central BHs in galactic nuclei. For lenses, ℓ makes equal excursions about zero, whereas loops maintain a definite sign of angular momentum. Eccentric discs, such as the one at the centre of M31, could well be composed of stars orbiting on the loop orbits of (3) above.

The aligned loops (which are fixed points of the slow dynamics) have constant angular momentum; ℓ is positive (negative) for anti-clockwise (clockwise) motion of the particle on its Keplerian ellipse. Their eccentricity, $e = d/a$, which means that the centres of the ellipses coincides with the centre of the perturbation (the BH is at one of the foci). For a fixed value of d, aligned loops of varying sizes (i.e. a), form a family of concentric, confocal ellipses. Not only can stars be placed on such orbits, but being a non–intersecting family, such nested ellipses can also be the streamlines of gas flows. Figure 5a shows one such representative set of aligned loops. Stable oscillations about these fixed point orbits allows ℓ to oscillate, while preserving a definite $\pm$ sign. Unlike the circulating loops of the centred perturbation (see Figure 1c), g for one of these *librating loops* oscillates about its mean value of π (see Figure 5b).

Tremaine (1995) has suggested that the nucleus of M31 is an eccentric disc in which stars move on nearly Keplerian orbits around a massive BH. In his model, the location of the BH coincides with the fainter (brightness) peak, P2, and brighter peak, P1, is the apoapsis region of the Keplerian ellipses. *We suggest that the aligned loop orbits (and their progeny, the librating loops) are the orbits that mostly make up Tremaine's eccentric disc.* If we imagine that the lopsided harmonic perturbation mocks self–gravity, our toy model suggests that the apsides of loop orbits can be trapped with favorable orientation. However, we do not expect details to carry over: for instance, we found that the aligned loop all shared a common centre. Such a property need not be true in general; indeed, extrapolating from Tremaine's simple, three–ring model, larger rings at the centre of M31 might be less displaced from the BH. We conjecture that quite general, three dimensional, lopsided perturbations will support aligned loops that can be used to build eccentric, thick discs.

4. Planar perturbations for general α

When $\alpha \neq 2$, it is no longer possible to obtain exact expressions for the slow Hamiltonian. One possibility is to evaluate H numerically, and study the contour plots. Another option is to look at limiting cases, which is what we do below. In this Section we study centred, nearly circular perturbations: $d_1 = d_2 = 0$ and $0 < \epsilon \ll 1$ Equation (11), for $\alpha \neq 0$, gives us the following

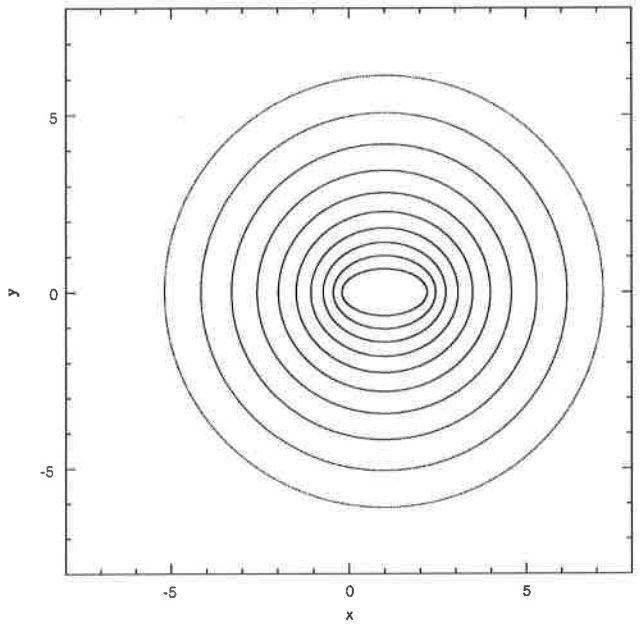

(*a*)

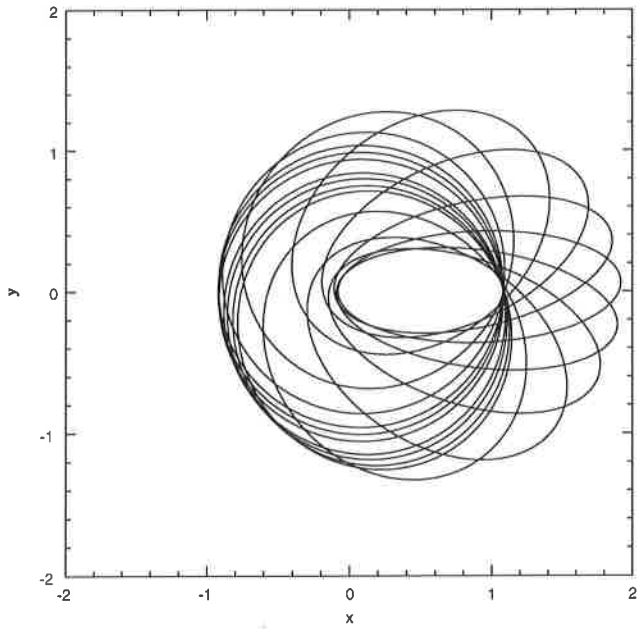

(*b*)

Fig. 5.— Loop orbits for the planar, lopsided, harmonic perturbation: (a) a set of aligned–loops when $d = 1$. The ten nested ellipses have $a = 1.2, (1.2)^2, \ldots, (1.2)^{10} \simeq 6.19$, (b) A librating loop for $d = 0.5$, $a = 1$, for which ℓ fluctuates between 0.4 and 0.97.

scale–free potentials:

$$\begin{aligned}\frac{\Phi(x,y)}{\mu I} &= \frac{1}{a^\alpha}\left(x^2+(1+\epsilon)y^2\right)^{\alpha/2} = \frac{1}{a^\alpha}\left(r^2+\epsilon y^2\right)^{\alpha/2} \\ &= \left(\frac{r}{a}\right)^\alpha + \epsilon\frac{\alpha}{2}\left(\frac{r}{a}\right)^{\alpha-2}\left(\frac{y}{a}\right)^2 + O(\epsilon^2)\,. \end{aligned} \tag{23}$$

We can now substitute in equation (23), the following expressions,

$$\begin{aligned} r &= a\left(1-\sqrt{1-\ell^2}\cos\eta\right)\,, \\ y &= a\left\{\sin\psi\,\left(\cos\eta-\sqrt{1-\ell^2}\right)+\ell\cos\psi\,\sin\eta\right\}\,, \end{aligned} \tag{24}$$

for r and y, and average over η to obtain the averaged Hamiltonian (see Appendix B for details of the derivation) correct to first order in ϵ:

$$\begin{aligned} H(\ell,\psi;\alpha,\epsilon) &= \left(1+\frac{\epsilon\alpha}{4}-\frac{\epsilon\alpha}{4}\cos 2\psi\right)F\left(-\frac{1+\alpha}{2}\,,\,-\frac{\alpha}{2}\,,\,1\,,\,1-\ell^2\right)\,+ \\ &+ \frac{\epsilon\alpha}{4}\,\ell^2\cos 2\psi\,F\left(\frac{1-\alpha}{2}\,,\,\frac{2-\alpha}{2}\,,\,2\,,\,1-\ell^2\right)\,+\,O(\epsilon^2)\,, \end{aligned} \tag{25}$$

where F is Gauss' Hypergeometric function. When $\alpha = 1$ or 2, the Hypergeometric series for F terminates, and the Hamiltonian assumes a simple form. We have already discussed the case $\alpha = 2$ in some detail.[7] When $\alpha = 1$,

$$\begin{aligned} F\left(-1,\,-1/2\,,\,1\,,\,1-\ell^2\right) &= \frac{3-\ell^2}{2}\,, \\ F\left(0,\,1/2\,,\,2\,,\,1-\ell^2\right) &= 1\,, \end{aligned} \tag{26}$$

so that

$$H(\ell,\psi,1,\epsilon) = \left(\frac{1}{2}+\frac{\epsilon}{8}\right)\left(3-\ell^2\right) - \frac{3\epsilon}{8}\left(1-\ell^2\right)\cos 2\psi + O(\epsilon^2)\,. \tag{27}$$

Figure 6a shows the isocontours of this Hamiltonian ($\alpha = 1$) for $\epsilon = 0.1$; as may be seen, these are similar to those of Figure 1a. Keeping ϵ small, we can vary α from -1 to 2. Figure 6b shows the isocontours for $\alpha = -0.9$; again the overall structure is unchanged. Hence we conclude that, for small ϵ, the orbital structure is independent of α in the range $(-1,2)$, with loops and short–axis lenses broadly similar to those in Figures 1b and 1c.

[7] For $\alpha = 2$, equation (25) reduces to equation (14), which happens to be an exact expression, because terms of $O(\epsilon^2)$ are identically zero for this case.

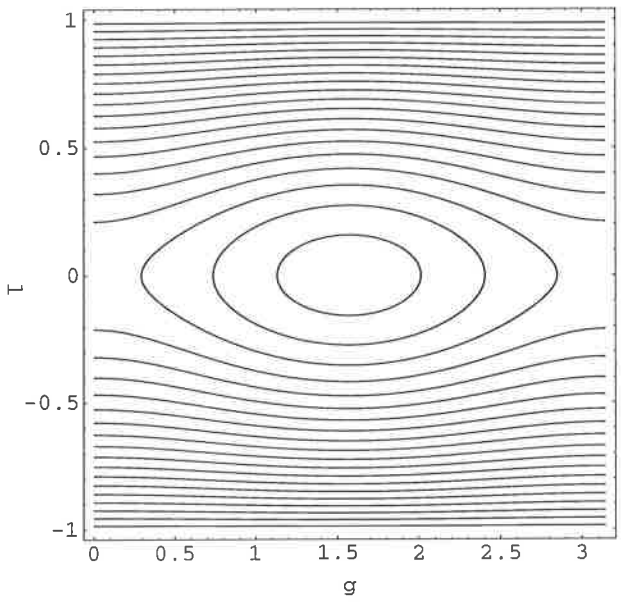

(*a*)

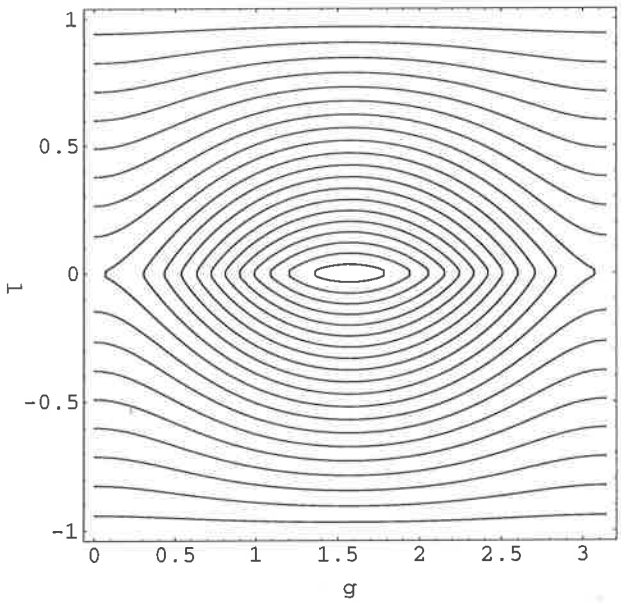

(*b*)

Fig. 6.— Isocontours of H for $\epsilon = 0.1$ (accurate to first order in ϵ): (a) $\alpha = 1$, (b) $\alpha = -0.9$.

5. The limits of averaging

The averaged Hamiltonian is an accurate proxy for the full Hamiltonian when the orbital period is much shorter than the period of precession of periapse. Such is mostly the case for orbits that evolve in the sphere of influence of the BH. However as one moves outwards, the influence of the perturbations relative to the BH's pull increases, the mismatch in frequencies decreases, thereby invalidating the averaging procedure. In practice, the breakdown occurs at resonances between orbital and precessional motion and is responsible for the emergence of minor orbit families such as the ones discussed by Gerhard and Binney (1985) and Miralda-Escude and Schwarzschild (1989)—hereafter GB and MES, respectively. GB were mostly interested in energetic orbits, far outside the sphere of influence, and give an incomplete picture of the orbits that live near the BH, claiming that "essentially all orbits in this regime are loop orbits". MES briefly discuss the effect of introducing a BH. In what follows, we collect results pertaining to dynamics in the combined potential of a BH and planar non-axisymmetric (possibly lopsided) potentials.

In keeping with history, we study the phase space of the logarithmic potential, with and without a central BH of mass M. The potential is

$$\Phi(x,y) = \frac{v_L^2}{2}\ln((x-d)^2 + \frac{y^2}{b^2} + R_c^2), \tag{28}$$

where v_L is the characteristic velocity of large loops, R_c is the core radius, b is a measure of non-axisymmetry, and d is the lopsidedness. The dynamics being two dimensional, we can explore the phase space structure on a Poincare section. In addition to the length scales, d and R_c, we have the radius of the sphere of influence of the BH, which is the radius at which the force exerted by the BH balances the force of the perturbing potential: $r_h = \mu^{1/3}R_c$ with, $\mu = \frac{GM}{R_c v_L^2}$.

5.1. The scale–free logarithmic potential

This case, for which $GM = R_c = d = 0$, was studied in detail by MES. Among other things, they identified families of resonant centrophobic orbits: banana, fish, pretzel...etc. The resonances are between the orbital period of the star and the period of precession of its pericentre. The banana for instance, performs two orbital revolutions in the time it takes its pericentre to precess once. For completeness, we redo MES's calculation. The potential is scale free and the motion has two degrees of freedom, so a single surface of section suffices to lay bare all the dynamics. Since we are interested in resonances between orbital and precessional motions, we choose to strobe the dynamics with the orbital period at each apocentre passage, recording the angular momentum, L, and the argument of the pericentre, g.

The resulting surface of section is shown in Figure 7. The phase space is divided between orbits with a definite sense of circulation (librating non-aligned loops and rosettes) and those

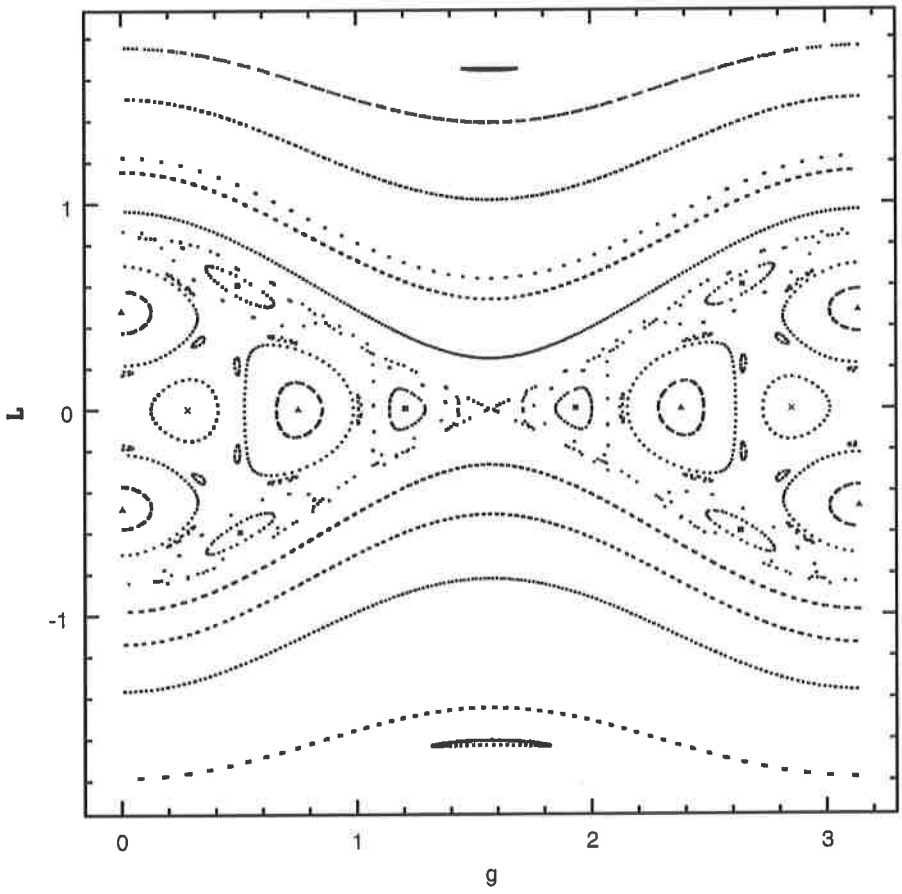

Fig. 7.— A Poincare section for the scale-free logarithmic potential when $b = 0.9$. The tori inside the separatrix are broken up into chains of islands corresponding to resonances. Marked are the banana (x), the fish (triangle), and the pretzel(square). One should also note the family of resonant, short axis loops.

with no definite sense of circulation. The later are split into resonant orbit families. The periodic orbit that engenders the banana family is caught at two pericentre passages, the fish at four and the pretzel at six. In this case, the period of precession of orbits is close to the orbital period, naturally precluding any averaging; the averaged picture would have missed this orbital structure (see Touma and Tremaine 1997 for a discussion of the averaged Hamiltonian). Following GB, it has been a common notion to think of box orbits being 'scattered' by the central cusp. We prefer to forget about boxes all together, and see these orbits as a natural outcome of resonant coupling between frequencies.

5.2. Adding a BH

Next, we stick a BH at the origin and watch the restructing of orbits that takes place. MES did introduce a BH but did not show any surface of section. They presented samples of high energy orbits, including some regular ones. With no core, the BH radius of influence is given by, $r_h = GM/v_L^2$. We measure distance in units of r_h, and look at sections of increasing energy. The energy is that of an orbit with zero velocity started on the x-axis, with $x = fr_h$, $f = 0.4, 2.0, 4.0$.

Within r_h (Figures 8a), the phase space is occupied by two main families of regular orbits: short axis lenses and loops. The lenses appear naturally in the integrable cusps with BHs presented in Sridhar and Touma (1997). The apparent integrability of the motion is consistent with the validity of averaging at distances where the motion is dominated by the BH. The phase space of the corresponding averaged Hamiltonian was not described previously in this paper, but it hardly differs from the averaged dynamics of centered harmonic perturbations discussed above (this should be obvious from the results of § 4). As one moves out in radius past r_h (Figure 8b), resonances become stronger, and a layer of stochastic motion develops near the separatrix. A torus has broken up into a chain of islands. The corresponding resonant periodic orbit, the bowtie, is shown in Figure 8c. Further away from the BH (Figure 8d), the short axis radial orbit becomes unstable, bananas are born, together with other resonant orbits families which overlap and lead to large scale chaos where once the regular lens orbits lived.

5.3. BH + logarithmic potential with core

The potential with a core is similar to the one considered by GB. They were mostly interested in energetic orbits far outside r_h and they find that, for nominal values, $b = 0.9$, $\mu = 0.02$, resonant orbit families and stochastic orbits dominate the phase space. When commenting on dynamics inside r_h, they just mention that most orbits are loops which, as we now know, is incomplete. We will follow the evolution from the nearly integrable motion described in § 3 to the breakdown of integrability.

Within r_h, we expect the potential to be well approximated by a harmonic core, and the

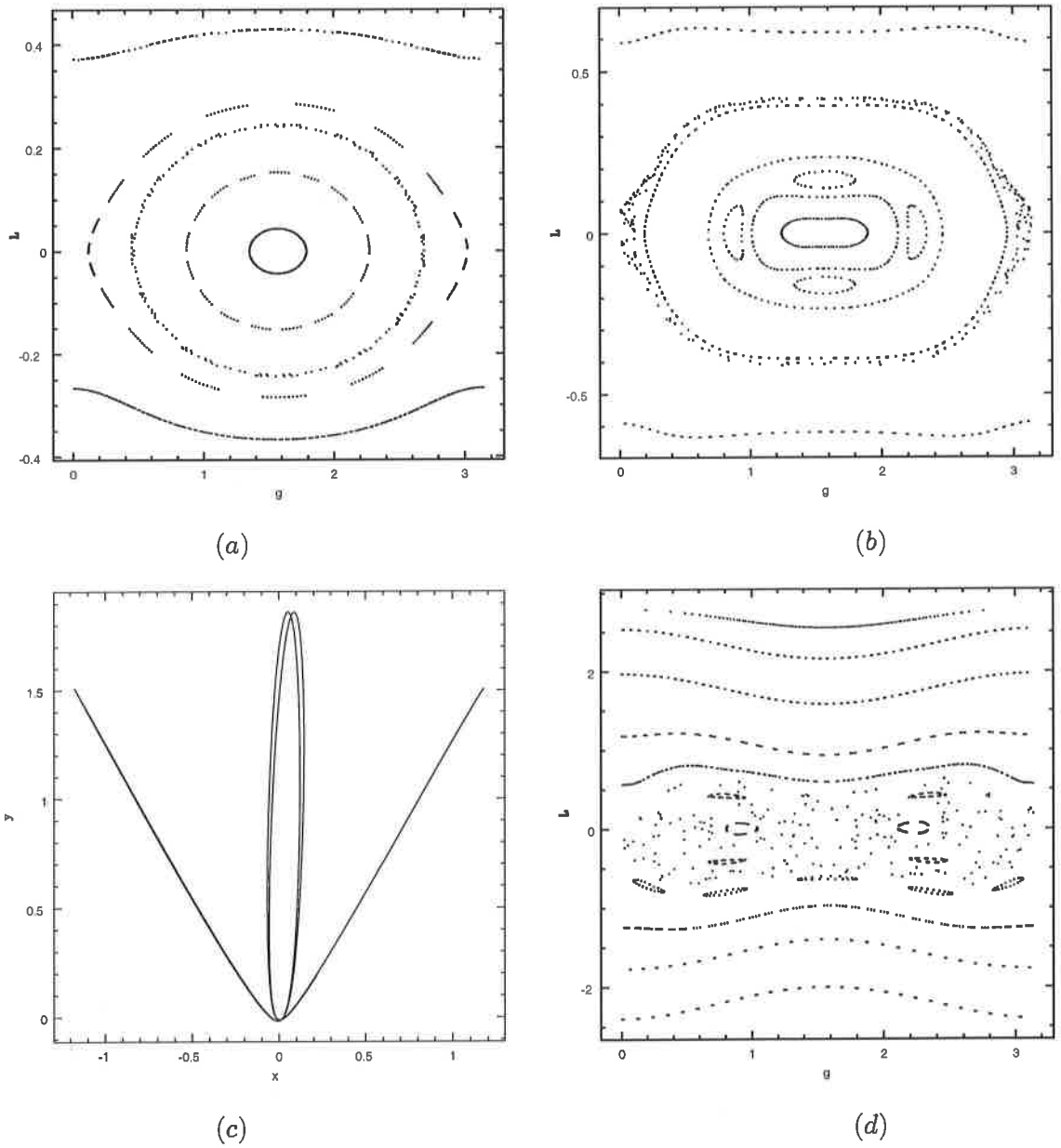

Fig. 8.— Dynamics in the potential of a black hole perturbed by a logarithmic potential with $b = 0.9$: (a) Section on energy surface with zero velocity orbit $y = 0$ and $x = 0.8r_h$; (b) similar section but with $x = 2.0r_h$; (c) Periodic orbit at the centre of the chain of islands seen in (b); (d) Section on energy surface with zero velocity orbit $y = 0$ and $x = 4.0r_h$.

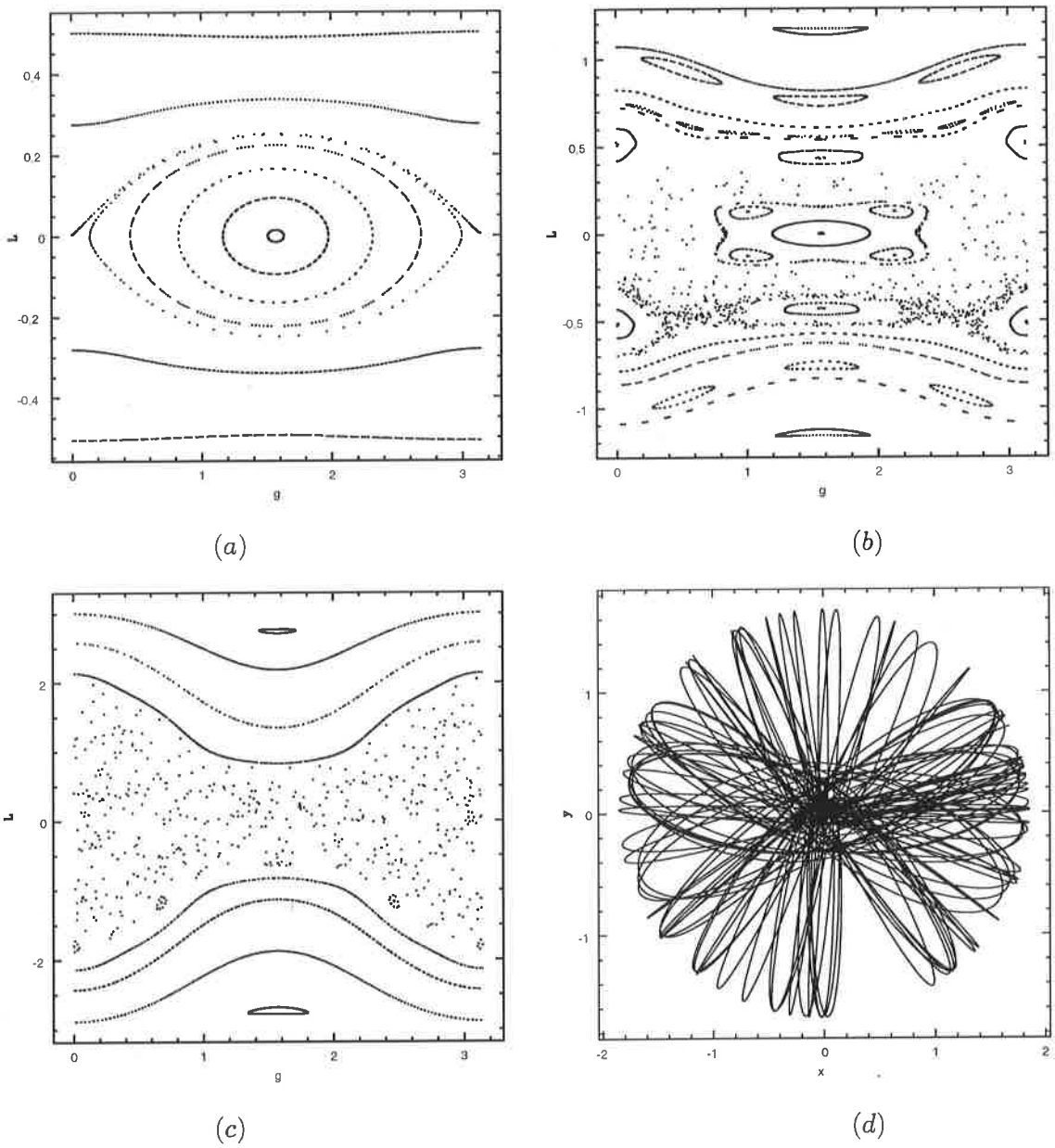

Fig. 9.— Dynamics in a logarithmic potential with core, $b = 0.9$, $\mu = 0.1$. Shown are sections on energy surfaces with zero velocity curve $y = 0$ and (a) $x = 1.0r_h$, (b)$x = 2.0r_h$, (c) $x = 4.0r_h$ and (d) a sample orbit from the stochastic sea in (c).

dynamics to be accurately described by the integrable, orbit averaged Hamiltonian. Indeed, as may be seen in Figure 9a, where we strobe orbits at edge of the sphere of influence, the phase space is regular with mainly short axis lenses and loops. As we progress outwards to $2r_h$, lenses and loops break down into resonant orbit families, which get stronger, overlap and lead to stochastic orbits. Regular lens orbits surround the stable short axis radial orbit. By $4r_h$, Figure 9c, the short axis radial orbit has gone unstable, regular lens orbits have disappeared, as the region within the separatrix is practically engulfed by a single stochastic orbit. A chaotic orbit at that same energy level is shown in Figure 9d. It explores all pericentre locations with neither a definite sense of circulation nor a definite sense of rotation. GB described stochasticity in terms of scattering. Here, it appears with the gradual sacrifice of regular orbits to resonances as we move away from the BH.

5.4. Lopsided logarithmic potential

Finally, we look at surfaces of section of a lopsided logarithmic potential, when $b = 0.9$, $d = 0.1R_c$, and $\mu = 0.1$. The sphere of influence has radius $r_h = 0.464R_c$. At $x = 0.4r_h$ (Figure 10a), $a \simeq 0.08$, $d/a > 1$: loops are absent, and aligned and anti-aligned lenses cover phase space; the regular orbit structure is consistent with averaging. For $x = 0.8r_h$ (Figure 10b), we are still within r_h, so we still expect the dynamics to be integrable. In this case $d/a < 1$; a family of aligned loops appears in a addition to the two families of lenses, in agreement with the averaged dynamics. For $x = 1.0r_h$, the dynamics is still quite regular. The aligned lenses have disappeared. The family of aligned loops is separated from the anti-aligned lenses by the usual loop orbits. By $x = 2r_h$, many resonant orbit families invade the phase space, and stochastic motion abounds around the separatrix. The central lens has lost its stability.

In conclusion, within the sphere of influence, the averaged Hamiltonian captures the orbit structure. The conditions for averaging break down outside the sphere of influence, and with it the regular orbit families of aligned loops and lenses, and anti-aligned lenses.

6. Discussion

In this paper we have introduced an averaging technique into the study of star clusters around massive BHs at the centres of galaxies. The dynamics of these clusters is governed by the combined gravitational potential of the central BH and the cluster itself. Within the sphere of influence (r_h) of the BH, the cluster potential is a small, yet non negligible perturbation. Orbits that are confined within r_h may be viewed as slowly precessing (and deforming) Keplerian ellipses. We have shown that these orbits possess a quasi–integral of motion, in addition to the energy integral; this nearly conserved quantity is $I = \sqrt{GMa}$, where M is the mass of the BH, and a is the semimajor axis of the orbit (when M is constant, the semimajor axis is nearly conserved). The

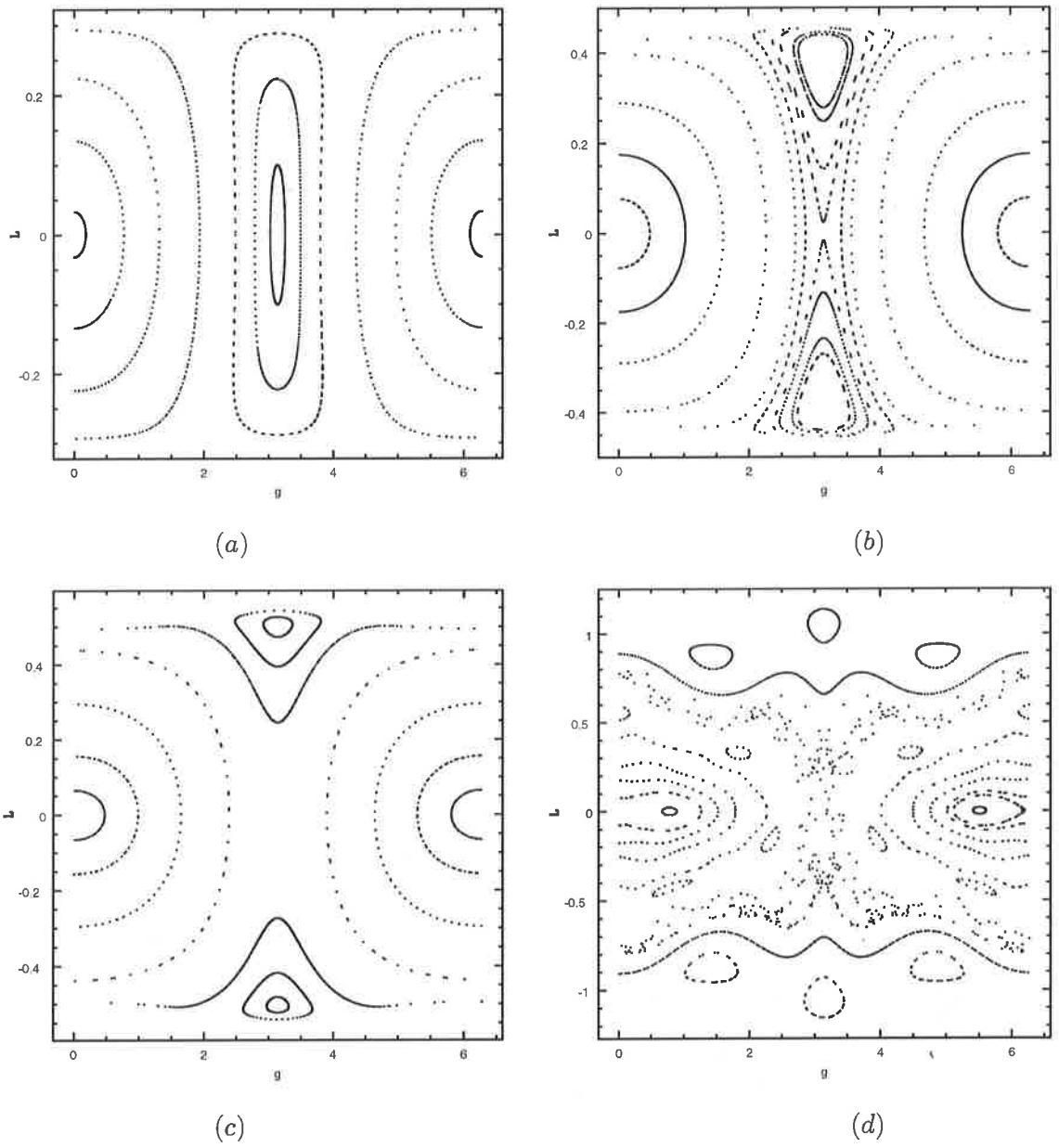

Fig. 10.— Surface of section for a lopsided logarithmic potential, with $b = 0.9$, $d = 0.1R_c$, $\mu = 0.1$, and increasing energy, determined by the zero velocity orbits, $y = 0$: (a)$x = 0.4r_h$, (b)$x = 0.8r_h$, (c) $x = 1.0r_h$, (d) $x = 2.0r_h$.

quasi–integral arises because the Keplerian orbital frequency is much larger than the frequencies of precessional motions. Taking advantage of this mismatch in frequencies, we averaged over an orbital period, to obtain a reduced dynamics of slow, precessional motions, wherein I appears as a full–fledged integral of motion.

The building of self–consistent stellar models for systems with low spatial symmetry (such as the central regions of M31 and NGC 4486B, which are known to possess double nuclei) surely requires the existence of more than one integral of motion. We now have in hand two integrals of motion—the energy and the semimajor axis—that may be used to construct dynamical models for the centres of galaxies like M31 and NGC 4486B. Let us verify that the conditions required for the averaging to apply are met in these two cases.

1. M31 probably has a central BH of mass $\sim 3 \times 10^7\,\mathrm{M}_\odot$. If we assume a central velocity dispersion $\sim 220\,\mathrm{km\,s^{-1}}$, then $r_h \sim 3\,\mathrm{pc}$ ($\sim 1''$). The double nuclei are separated by $\sim 0.''5$ arcsec, and much of the nuclear disc itself appears to be within r_h. Furthermore, within $1''$, the mass of the disc and the bulge are only 16 %, and 2 % of the mass of the BH respectively (see Tremaine 1995). Within r_h, the gravitational potentials of the disc and the bulge are small, but non negligible, perturbations to the potential of the BH; indeed, this is a situation that is ripe for the application of the averaging technique! In § 3.2 and 3.3, we considered orbits in a toy model of a lopsided perturbation, and discovered that there are a very interesting class of loop orbits that are elongated in the same sense as the perturbation. The existence of these aligned loop orbits is an encouraging sign that Tremaine's (1995) eccentric disc can be realised as a self–consistent model.

2. NGC 4486B (a low luminosity E1 companion of M87) also has a double nucleus separated by $0.''15$ (Lauer et.al. 1996). There seems to be some evidence for a central BH of mass $\sim 6 \times 10^8\,\mathrm{M}_\odot$ (Kormendy et. al. 1997). For an assumed central velocity dispersion $\sim 280\,\mathrm{km\,s^{-1}}$, and an assumed distance to NGC 4486B of 16 Mpc, we estimate that $r_h \sim 0.''48$, length scale that is not only larger than the separation between the nuclear peaks, but also one that is nearly five times larger than than the best resolution obtainable with the HST; hence the averaging technique may be expected to be useful here too. Kormendy et. al. (1997) suggest that the double nucleus might arise from a stellar distribution similar to Tremaine's (1995) disc. However, as Lauer et.al. (1996) note, there are differences from the case of M31, and even the evidence for a massive BH is less certain.

A fundamental result of this paper is that, relativistic effects apart, the presence of a massive BH enforces a certain degree of integrability within its sphere of influence; and this happens because of the extra quasi–integral, I. Even without detailed knowledge of the (perturbing cluster) potential, we were able to note that slow dynamics in (i) razor–thin discs is fully integrable because the problem is two dimensional, (ii) any axisymmetric potential is fully integrable (note that axisymmetry allows for lopsidedness), and (iii) a potential with no spatial symmetry whatsoever still conserves two integrals, so that any precessional chaos must be highly limited in nature.

When the potential is time dependent, but with variation occurring over times longer than the orbital times, averaging is still applicable. We discussed the case of the adiabatic growth of the BH. Another case of slow time variation comes to mind: this is the 'resonant relaxation' of Rauch and Tremaine (1996), a process that relies on Two body encounters between stars. The time scales are typically much longer than orbital times, so averaging applies, and the stars in their courses may be treated as elliptical rings. Over certain time scales (shorter than the classical two body relaxation times), the semimajor axes of all the stars are approximately constant, whereas torques between the rings exchange angular momentum. As the authors note, this can lead to a situation in which some regions of nuclear star clusters are relaxed in angular momentum, but not in energy.

We introduced a family of model potentials for this case, that allowed for a range of cusp slopes (α), non–axisymmetry and lopsidedness, with a view to classification of orbit families. For the harmonic case ($\alpha = 2$), we showed that centered non–axisymmetric perturbations support two main families of orbits: short axis lenses and loops. Lenses were already identified in Sridhar and Touma (1997) and should be recognized as an essential feature of regular motion around BHs. They have zero average angular momentum and fill out lens shaped regions in configuration space. The loops are the familiar rosettes of slightly perturbed Keplerian motion. We explored the consequence of lopsidedness and watched the emergence of a family of (resonant) aligned loops whose elongation is in the same sense as the lopsidedness, a property which makes them ideal candidates for the construction of eccentric disks and describing double nuclei in the manner suggested by Tremaine (1995).

When $\alpha \neq 2$, the case of small non–axisymmetry ($\epsilon \ll 1$) is analytically tractable. It is interesting to note that the qualitative nature of the orbits (lenses and loops) appears to be insensitive to α. This is probably because the force exerted on a star due to the perturbing potential—even when it becomes infinitely large at the centre—is overwhelmed by the force due to the BH. If such is the case for larger non–axisymmetry, then our explorations of the harmonic case provide a sketch of the possible orbit families in razor–thin discs around massive BHs. Whether the qualitative nature of dynamics around BHs is indeed independent of the steepness of the cusp in density is an unsolved problem, but one that is tractable by methods such as our averaging technique.

Averaging is of course valid as long as we are away from resonances—in this case between the orbital period and the period of precession of periapse or the node. We showed, numerically, that such a condition is satisfied within r_h, and breaks down outside. Orbits which take a star far outside r_h may be expected to be chaotic, as explored in the works of Merritt and collaborators. Central BHs and strong cusps might force the main body on an elliptical galaxy to evolve toward axisymmetry. However, as we have argued in this paper—and reinforced by the examples of M31 and NGC 4486B—we suggest that the central regions of a galaxy can stubbornly persist with their striking variety of non–axisymmetric features.

7. ACKNOWLEDGMENTS

We thank the Raman Research Institute, and the Indian Railways for their hospitality while this work was in progress. JT wishes to thank IUCAA for support and hospitality at Pune, as well as acknowledge the support of the Harlan Smith Fellowship under NASA grant NAGW 1477.

A. The case $\epsilon = 3$

We show that the *unaveraged* dynamics, in the combined potential of a BH and a centered harmonic perturbation, is integrable, when $\epsilon = 3$, or $b = 0.5$. Indeed the combined potential,

$$\Phi = -\frac{GM}{\sqrt{x^2+y^2}} + K(x^2+4y^2), \tag{A1}$$

when expressed in parabolic coordinates (see Sridhar and Touma 1997 for details), $\xi = y+\sqrt{x^2+y^2}$, and $\eta = y - \sqrt{x^2+y^2}$, takes the form

$$\Phi = \frac{F_+(\xi)}{\xi-\eta} + \frac{F_-(\eta)}{\eta-\xi}, \tag{A2}$$

where

$$\begin{aligned} F_+(\xi) &= K(\xi^3 - GM) \\ F_-(\eta) &= K(-|\eta|^3 + GM)\,. \end{aligned} \tag{A3}$$

This form is that of a separable, Stäckel potential in parabolic coordinates, which supports integrable motion.

B. Derivation of equation (25)

Let Φ denote the potential given in equation (23). Substitute for r and y, the expressions given in equations (24), and average over η in the usual manner. This gives us the averaged Hamiltonian, $H = (\overline{\Phi}/\mu I) = H_0 + \epsilon H_1 + O(\epsilon^2)$, where

$$\begin{aligned} H_0 &= \frac{1}{2\pi}\oint d\eta \left(1-\sqrt{1-\ell^2}\cos\eta\right)^{\alpha+1}, \\ H_1 &= \frac{\alpha}{4\pi}\oint d\eta \left(1-\sqrt{1-\ell^2}\cos\eta\right)^{\alpha-1} \times \\ &\quad \times \left\{\sin\psi\left(\cos\eta - \sqrt{1-\ell^2}\right) + \ell\cos\psi\right\}^2. \end{aligned} \tag{B1}$$

Some straightforward algebra allows us to express

$$H = \left(1+\frac{\epsilon\alpha}{4}\right)A(\ell;\alpha) - \frac{\epsilon\alpha}{4}B(\ell;\alpha)\cos 2\psi \;+\; O(\epsilon^2)\,, \tag{B2}$$

in terms of the two functions, A and B:

$$\begin{aligned} A(\ell;\alpha) &= \mathcal{I}\left(\sqrt{1-\ell^2}\,,\,\frac{3}{2}+\alpha\,,\,0\right) \\ B(\ell;\alpha) &= A(\ell;\alpha) - 2\ell^2\,\mathcal{I}\left(\sqrt{1-\ell^2}\,,\,\frac{1}{2}+\alpha\,,\,1\right), \end{aligned} \tag{B3}$$

where

$$\begin{aligned} \mathcal{I}(e;\lambda,\nu) &\equiv \frac{1}{2\pi}\oint d\eta\,(1-e\cos\eta)^{\lambda-\nu-1/2}\,\sin^{2\nu}\eta \\ &= \frac{\exp(\lambda-\nu-1/2)}{\pi}\int_0^\pi d\eta\left(\frac{1}{e}+\cos\eta\right)^{\lambda-\nu-1/2}\sin^{2\nu}\eta \\ &= \frac{1}{\sqrt{\pi}}\frac{\Gamma(\nu+1/2)}{\Gamma(\nu+1)}\,F\left(\frac{2\nu-2\lambda+1}{4},\,\frac{2\nu-2\lambda+3}{4},\,\nu+1\,,\,e^2\right), \end{aligned} \tag{B4}$$

where the last identity involving the Hypergeometric function, F, is obtained by using formulae 3.666, 8.703 and 9.131 (1) of Gradshteyn and Ryzhik (1994). Then

$$\begin{aligned} A(\ell;\alpha) &= F\left(-\frac{1+\alpha}{2}\,,\,-\frac{\alpha}{2}\,,\,1\,,\,1-\ell^2\right), \\ B(\ell;\alpha) &= A(\ell;\alpha) - \ell^2\,F\left(\frac{1-\alpha}{2}\,,\,\frac{2-\alpha}{2}\,,\,2\,,\,1-\ell^2\right) \end{aligned} \tag{B5}$$

Substituting for A and B in equation (B2) completes the derivation.

REFERENCES

de Zeeuw, P.T., 1985, MNRAS, 216, 273

Gebhardt, K., Richstone, D., Ajhar, E. A., Lauer, T. R., Byun, Y.-I., Kormendy, J., Dressler, A., Faber, S. M., Grillmair, C., and Tremaine, S., 1996, AJ 112, 105

Gerhard, O. E., & Binney, J., 1985, MNRAS 216, 467

Goldstein, H., 1980, Classical Mechanics, 2nd ed. (Reading: Addison-Wesley)

Gradshteyn, I. S., and Ryzhik, I. M. 1994, Table of Integrals, Series, and Products, edited by A. Jeffrey (Academic Press, Inc, Boston)

Hagihara, Y., 1971, Celestial Mechanics II, Part I (MIT Press, Cambridge, Ma)

Kormendy, J., 1982, in Morphology and Dynamics of Galaxies, edited by L. Martinet and M. Mayor (Geneva Observatory, Sauverny), p 113

Kormendy, J., 1987, in Structure and Dynamics of Elliptical Galaxies, IAU Symposium No. 127, edited by T. de Zeeuw (Reidel, Dordrecht), p 17

Kormendy, J., & Richstone, D., 1995, ARAA 33, 581

Kormendy, J., Bender, R., Magorrian, J., Tremaine, S., Gebhardt, K., Richstone, D., Dressler, A., Faber, S.M., Grillmair, C., Lauer,T.R., 1997, ApJ, 482, L139

Lauer, T.R., 1983, Ph.D thesis, University of California, Santa Cruz

Lauer, T.R., 1985, ApJ, 292, 104

Lauer, T.R. et. al. 1993, AJ, 106, 1436

Lauer, T.R., Ajhar, E.A., Byun, Y.I., Dressler, A., Faber, S.M., Grillmair, C., Kormendy, J., Richstone, D.O., Tremaine, S., 1995, AJ, 110, 2622

Lauer, T.R., Tremaine, S., Ajhar, E.A., Bender, R., Dressler, A., Faber, S.M., Gebhardt, K., Grillmair, C.J., Kormendy, J., Richstone, D.O., 1996, ApJ, 471, L79

Merritt, D., 1996, Science 271, 337

Merritt, D., & Fridman, T., 1996, ApJ 460, 136

Merritt, D., & Valluri, M.. 1996, ApJ 471, 82

Miralda-Escudé, J., & Schwarzschild, M., 1989, ApJ 339, 752

Peebles, P.J.E., 1972, Gen. Rel. Grav., 3, 61

Plummer, H. C., 1960, An Introductory Treatise on Dynamical Astronomy (Dover, New York)

Rauch, K.P., & Tremaine, S., 1996, New Astronomy, 1, 149

Rees, M.J., 1990, Science, 247, 817

Sridhar, S., & Touma, J., 1997, MNRAS 287, L1-L4

Touma, J. & Tremaine, S., 1997, MNRAS 292, 905

Tremaine, S., 1995, AJ, 110, 628

Young, P., 1980, ApJ, 242, 1232